European Polymer Journal 45 (2009) 2288–2303

Contents lists available at ScienceDirect

European Polymer Journal

journal homepage: www.elsevier.com/locate/europolj

Predictive control and verification of conversion kinetics and polymer molecular weight in semi-batch free radical homopolymer reactions

Tomasz Kreft, Wayne F. Reed *

Physics Dept., Tulane University, New Orleans, LA 70118, USA

ARTICLE INFO

Article history:
Received 20 January 2009
Received in revised form 26 March 2009
Accepted 6 May 2009
Available online 10 May 2009

Keywords:
Polymerization kinetics
Reaction monitoring
Reaction control
Light scattering
Polymer characterization

ABSTRACT

Polymer molar mass distributions critically affect macroscopic characteristics and performance of polymeric materials. While multi-detector methods coupled to size exclusion chromatography (SEC) are widely used to measure endproduct mass distributions, less progress has been made in simultaneously controlling and verifying the evolution of these distributions during synthesis. This work focuses on quantitative predictions and online verification of conversion kinetics and of molecular weight during free radical homopolymerization of acrylamide, where reagents were fed into the reactor during the reaction. The central task is to establish and experimentally test a formalism combining free radical polymerization kinetics with time dependent processes related to flows of material into and out of the reactor. Monomer feed experiments were performed that alternately hold molecular weight constant and ramp the weight up, in contrast to batch reactions, where molecular weight decreases. Three types of initiator feed 'tapers' were also used to produce predictable conversion kinetics and mass distributions: (i) constant initiator feed, (ii) linearly stepped feed to produce Gaussian conversion kinetics, and (iii) booster shots to produce multi-modal masses. Automatic Continuous Online Monitoring of Polymerization reactions (ACOMP) was used to follow the conversion and evolution of the average mass distribution, and multi-detector SEC was used to cross-check results and measure full distributions of endproducts. In general, there was good agreement between the predictions and results. In future work this approach can be used as an Ansatz for reaction trajectory prediction, and the online monitoring signals exploited to make feedback controlled corrections to the reagent flows and other reaction conditions.

1. Introduction

As demand for new and more sophisticated polymers increases, there must be corresponding developments for controlling the polymerization reactions themselves, especially as regards control of the polymer molecular weight. Full, feedback control of reactors for small molecules has been available for many years. For polymer reactions, however, the state of the art is less advanced, because, despite numerous and deep works on the mathematical theory, most *in situ* sensors, such as infrared (IR) and Raman scattering, primarily measure monomer conversion, not polymer molar mass. Rheological measurements inside of reactors provide a link to polymer molecular weight, but not a direct measurement.

The lack of on-line measurement of polymer properties is usually the main problem in closed-loop control of polymerization reactions. For that reason many open-loop methods have been applied. The controllers employed in closed-loop methods use some on-line measurements, but heretofore none have continuous streams of conversion and molecular weight data available. Hence control, still heavily depends on the accuracy of available mathematical models for the input parameters.

* Corresponding author.
E-mail addresses: tkreft@tulane.edu (T. Kreft), wreed@tulane.edu (W.F. Reed).

0014-3057/$ - see front matter © 2009 Elsevier Ltd. All rights reserved.
doi:10.1016/j.eurpolymj.2009.05.006

Automatic Continuous Online Monitoring of Polymerization reactions (ACOMP) allows comprehensive, model-independent monitoring of monomer and comonomer conversion, weight average molar mass M_w, weight average intrinsic viscosity $[\eta]_w$, average composition drift and distribution (for copolymers), and certain measures of polydispersity [1,2]. ACOMP hence provides all the necessary on-line measurements for closed-loop control.

While full feedback control based on ACOMP is a long-term goal, this work takes the first step in this direction by employing predictive control. In this, the kinetic data provided by ACOMP are used to develop semi-batch polymerization reaction processes with predictable trends in conversion and M_w, and the predictions are verified during the reactions.

There is extensive work on measuring, controlling and engineering more robust polymerization reactors, concisely summarized by Richards and Congalidis [3]. As they report, much attention has been devoted to maintaining pressure, temperature, level and flow (PTLF) in the reactor [4,5]. Different online composition measurement techniques, such as IR analysis [7], Fourier transform infrared (FTIR), near IR (NIR) [40], Raman spectroscopy [6], calorimetry [7], and gas chromatography [7] are available.

There has been a significant amount of work reported on controlling composition during copolymerization reactions. The Kalman filter method is based on a linear approximation of the nonlinear process [8] but has problems with stability and convergence [9–13]. For that reason, numerous nonlinear methods have been developed. Ellis et al. [10] proposed an extended Kalman filter that has been used for control purposes [12,13]. Nonlinear state observers that use rate of heat generation due to chemical reaction were used by Hammouri et al. [8] to obtain key parameters during free radical copolymerizations. These estimations and techniques are simpler to tune than Kalman filters [14,15]. Kravaris et al. [16] used temperature tracking as another nonlinear method to control copolymer composition. Model predictive control (MPC) [17,18], as well as nonlinear MPC (NLMPC) [19–22] algorithms have been suggested for control of nonlinear systems.

The semi-batch approach, where policies are developed for selective reagent feeds to the reactor has been extensively elaborated, especially for emulsion polymerization, and in the context of controlling composition during copolymerization reactions [8,21,23–27,31]. Sun et al. developed model based semi-batch monomer feeding policies for controlled radical polymerization (CRP) [28,29]. They provided a reactor model with mass balance equations and showed experimental results of controlling the composition. Vicente et al. [30,31] controlled composition and molecular weight distribution in emulsion copolymerization in an open-loop method by maintaining the ratio of comonomers. Yanjarappa et al. [32] synthesized, via a semi-batch method, copolymers with constant composition for biofunctionalization. General semi-batch policies are reviewed by Asua [33].

One of the biggest issues in reactor control is the problem of nonlinearities arising during the reaction due to gelation, cage effects, exothermicity, drastic changes in kinetic coefficients (e.g. propagation and termination coefficients), etc.

The focus of the current work is to control molecular weight and conversion kinetics for free radical homopolymerization. There have been efforts to control molecular weight, such as those by Kiparissides et al. [34], Othman et al. [15], Wu and Shan [26]. It is frequently reported that the main difficulty in controlling the molecular weight is the lack of on-line sensors.

In general the best way to control molecular weight is by manipulating the concentration of monomer, initiator, or chain transfer agent [15,35–40]. Modi and Guillet [41] described a photochemical method using a 1,3-(di-1-naphtyl)propan-2-one (DNP) compound. In the presence of DNP, when exposed to light, growing polymer chains during a free radical polymerization reaction are terminated, hence providing a means to control molecular weight, even if not particularly effective.

In the past the molecular weight was often controlled by temperature [42]. Many problems with this approach have been reported [3,8,14,15,17]. Garcia [43] employed MPC for semi-batch polymerization where the reactor temperature was controlled by monomer addition and cooling water. The use of temperature as the only parameter to control molecular weight can succeed only for a limited molecular weight range. Alhamad et al. [17] used a multivariable MPC in emulsion polymerization to control the particle size and molecular weight distribution (MWD) by manipulating the flow rates of monomers, surfactant, initiator and temperature of the reactor. They used off–line chemical solutions as set points for the MPC control. The set points were sent to the plant then, due to lack of on-line sensors, conversion, average particle size, molecular weight, etc. were estimated by a "soft sensor", which is a real-time, predictive simulation that uses knowledge of current reactor conditions such as flow rates and temperature. As a result they were able to achieve more degrees of freedom and hence a tighter control of molecular weight.

Again, due to problems with on-line measurements, Vicente at al. [30] controlled composition and MWD in emulsion copolymerization by an open-loop semi-batch method. They computed optimal feed profiles using iterative dynamic programming. The success of this method depends on how good the mathematical models are and requires that there be no unmodeled disturbances during the process. They estimated conversion from calorimetric data. Off-line measurements after the reaction agreed with the estimations and confirmed that the mathematical model was good. The authors admitted, however, that more robust closed-loop methods involving on-line measurements would have to be developed for better control.

Othman et al. [15] proposed a closed-loop method to control molecular weight. They used NIR to estimate conversion. They developed a nonlinear estimator to get the reaction rate necessary for the control loop. This method relies on the quality of offline measurements necessary for NIR calibration. They used non-linear high gain observers to identify model parameters and the reaction rates which were used to obtain desired monomer feeds to keep M_w constant. This feedback control produced high molecular masses which could not be achieved in

open-loop cases but the approach still relies on the quality of the model.

Hur et al. [27] designed a multivariable model-on demand predictive controller (MoD-PC) that overcomes the imperfections of other identification methods in controlling molecular weight and composition during semi-batch copolymerization. In this simulation they also used reaction temperature and the feed flow rates as variables to be manipulated and molecular weight and composition as the control outputs. The strength of the designed MoD-PC simulation lies in the fact that it identifies a model using data belonging to a small neighborhood around the current operating point rather than estimating a complex global model.

Park and Rhee [19] used a learning-based nonlinear model predictive control (NLMPC) to control semi-batch copolymerization. The purpose was to linearize a nonlinear model based on previous batch data. In this way the prediction is a function of the increment of inputs between two consecutive batches. They used an online densitometer to obtain conversion and a viscometer to calculate molecular weight. These measured properties were fed back, and, by using estimation and optimization procedures, the necessary feeds were obtained. Simulations were successful and were experimentally verified for a methacrylate/methyl acrylate copolymerization. The system did not exhibit any disturbances for any reaction. As the authors report, in general, disturbance models will have to be used for successful control.

In the following, a compact formalism for extracting the primary quantities from the ACOMP detector train is first presented, and then a number of process scenarios are predicted, carried out experimentally, and assessed by online measurements. The emphasis is on the developing and testing formalisms that combine the time dependence of natural free radical polymerization kinetics and reagent flows.

It is important to point out that, although, in the following formalism, no disturbances to flow are taken into account, such disturbances, e.g. in reagent flow rates due to possible blockages or pump performance issues, will be immediately detectable in the continuous ACOMP signals; for example, if monomer is being fed into the reactor and a blockage slows or stops the flow rate, all the signals – light scattering, viscosity, refractive index, and UV absorption – will show an abrupt change in their trends, alerting the reaction operator to the problem; i.e. the online monitoring itself, without any models, formalism, or interpretation quickly detects anomalies.

2. Formalism for combined reaction and semi-batch flow

ACOMP continuously extracts, dilutes, and conditions the reactor contents, so that the detectors report the cumulative state of the reaction; i.e. the current concentrations of monomer and polymer, M_w and $[\eta]_w$. From the continuous record of these properties, it is also possible to compute instantaneous values of M_w and other quantities. The delay time between extraction and measurement in the detector train is typically on the order of tens of seconds to a few minutes. Composition drift, average composition, and reactivity ratios can be found in the case of free radical [44] and living gradient copolymerization [45].

Here, expressions are first derived for the concentration of monomer and polymer in the reactor, while reactions are occurring, when N solutes in solution are allowed to flow into the reactor, each at their own rate, which need not be constant, such that solute s has caused a change in reactor volume at time t of $\Delta V_s(t)$, where $Q_s(t)$ is the instantaneous flow rate of liquid from a reservoir containing component s into the reactor. In the following a constant withdrawal rate from the reactor q (cm^3/s) that feeds the ACOMP extraction/dilution/conditioning front end is assumed, which in turn provides a continuous flow of dilute polymer solution to the detector train. The extraction flow rate q is in lower case to indicate that it is normally quite low, on the order of 0.01–0.2 cm^3/minute, and is intended to be a non-perturbative extraction stream. Usually, the effect of the ACOMP withdrawal from the reactor can be ignored, although for lengthy reactions in small volume reactors the effects can become important.

The detectors provide the signals that allow monomer and polymer concentrations in the reactor to be measured during the reaction and under inflow of N solutes, and are combined with light scattering and viscosity signals to compute M_w and $[\eta]_w$. Since q is constant the ACOMP front end will maintain a constant dilution factor, d, so that the concentrations of any solute, s, in the reactor, $c_s(t)$, will be measured in the detector train as $dc_s(t)$.

Because volume and concentrations in the reactor are changing, it is best to work on the basis of the mass balance of component s in the reactor, $m_s(t)$, measured in grams. Then, the rate at which $m_s(t)$ changes is

$$\frac{dm_s}{dt} = c_s\prime Q_s(t) - \frac{m_s}{V(t)}q - \varepsilon_s(t) + \gamma_s(t) \tag{1}$$

c_s' is the concentration of s in the reservoir from which it is being pumped into the reactor at rate $Q_s(t)$, $\varepsilon_s(t)$ is the rate at which m_s is lost due to any reactions, and $\gamma_s(t)$ is the rate at which s is produced by any reactions. $V(t)$ is the total volume in the reactor, and is given by

$$V(t) = V_0 - qt + \sum_{s=1}^{N}\int_0^t Q_s(t')dt' \tag{2}$$

where the partial volume change due to each flowing solute s is

$$\Delta V_s(t) = \int_0^t Q_s(t')dt' \tag{3}$$

The concentration of any solute s at any time is hence

$$c_s(t) = \frac{m_s(t)}{V(t)} \tag{4}$$

In this work v_s is the constant relating mass concentration of solute s, c_s (g/cm^3), to molar concentration of s, $[s]$ (mol/L)

$$c_s = v_s\,[s] \tag{5}$$

v_s is given by $v_s = 10^{-3} \times M_s$, where M_s is the molecular weight of s. For acrylamide (Am) $v_A = 0.07108$ g L/cm^3 mol,

and for potassium persulfate (KPS) v_{KPS} = 0.27032 g L/cm^3 mol.

2.1. Effect of reactor inflow and outflow on concentration of any solution components

The mere act of extracting liquid and injecting component-containing liquids into the reactor can alter mass and concentrations. Consider how the molar concentration of component s, $[s]$, changes due purely to flow

$$\frac{d[s]}{dt}_{Flow} = \frac{1}{v_s V(t)}\frac{dm_s}{dt} - \frac{m_s}{v_s V(t)^2}\frac{dV(t)}{dt} \tag{6}$$

The rate at which m_s changes due to flow is

$$\frac{dm_s}{dt}_{Flow} = c_s' Q_s(t) - q\frac{m_s}{V(t)} \tag{7}$$

Taking the time derivative of Eq. (2), and combining this with Eqs. (6) and (7) yields

$$\frac{d[s]}{dt}_{Flow} = \frac{c_s' Q_s(t)}{v_s V(t)} - \frac{c_s}{v_s V(t)}\sum_j Q_j(t) \tag{8}$$

The first feature to note here is that the continuous extraction of liquid from the reactor by the ACOMP 'front-end' at rate q does not change the concentration of any of the components when there are no flows $Q_s(t)$ into the reactor (i.e. $Q_s(t) = 0$ for all s), so that pure batch formulations are used for ACOMP in which the only flow is extraction from the reactor at any rate q.

Another feature of Eq. (8) is that the concentration of any component s will be held constant in the absence of reactions if

$$c_s' Q_s(t) = c_s \sum_j Q_j(t) \tag{9}$$

If one wishes to hold the concentration of *all* components constant, then the two limiting cases for this are to use a single reservoir pumping into the reactor at rate $Q(t)$, or to use a separate reservoir for each component, each pumping into the reactor at rate $Q_s(t)$.

In the case of a single reservoir, $Q(t) = \sum_j Q_j(t)$, but since $c_s' Q(t) = c_s \sum_j Q_j(t)$ by Eq. (9), $c_s' = c_s$ for all components; i.e. the concentration of the reactor can only be held constant while being fed from a single reservoir if the concentration of each component in the reservoir is the same as in the reactor itself.

For multiple reservoirs, Eq. (9) is satisfied for each component, and each component has its own flow rate $Q_s(t)$ from its reservoir, which requires

$$\sum_s Q_s(t) = \sum_s \frac{c_s}{c_s'}\sum_j Q_j(t) = \sum_j Q_j(t) \tag{10}$$

leading to the condition that

$$\sum_s \frac{c_s}{c_s'} = 1 \tag{11}$$

i.e. one can independently establish the flow rate Q_s from each reservoir, then use Eq. (9) to compute c_s/c_s', which will then also satisfy Eq. (11).

2.2. Free radical batch polymerization kinetics and molecular weight considerations

This section treats batch kinetics, which are subsequently modified in succeeding sections to account for reagent and solvent flows into and out of the reactor.

Traditionally, free radical polymerization kinetics is divided into the (i) initiation, (ii) propagation, and (iii) termination stages, and quantitative kinetics can be obtained analytically, e.g. via the Quasi Steady State Approximation (QSSA) [47], or by numerically integrating the rate equations. The kinetic equations used here follow the convention of reference [46] as concerns factors of '2' in radical balance and kinetic chain length equations. This convention has been used consistently throughout this group's ACOMP publications.

The initiation step in forming initiated radicals $R_1\bullet$ is determined by two reactions, the initiator decomposition,

$$I_2 \xrightarrow{K_d} 2I\bullet \tag{12a}$$

where k_d is the temperature dependent first-order decomposition rate coefficient, and the bimolecular reaction

$$I\bullet + m \xrightarrow{K_i} R_1\bullet \tag{12b}$$

where k_i is the initiation rate coefficient. Production of $I\bullet$ in Eq. (12a) proceeds according to

$$[I_2] = [I_2]_0 \exp(-k_d t) \tag{13}$$

Either of the two reactions (12a) and (12b) above can be rate controlling, and the rate controlling reaction will in turn affect the propagation rate equation (k_p is the propagation rate coefficient),

$$\frac{d[m]}{dt} = -k_p[m][R\bullet] \tag{14}$$

via the controlling mechanism's effect of how $[R_1\bullet]$ depends on $[m]$; If the monomer is very dilute the diffusion controlled reaction (Eq. (12b)) will be rate limiting, and so $[R_1\bullet] \propto [m]^{1/2}$ under the QSSA, whereas for higher monomer concentrations the initiator decomposition (Eq. (12a)) is rate controlling, in which case $[R_1\bullet]$ is independent of $[m]$ under the QSSA, so that monomer conversion is a simple first-order (exponential) process. Eq. (14) is the long chain limit in the QSSA. For the degree of polymerization of polymers in this work ($N \gg 100$), this is an excellent approximation.

This foregoing is summarized by considering the mass balance of the entire population of radicals $[R\bullet] = \sum_i [R\bullet]_i$

$$\frac{d[R\bullet]}{dt} = 2Fk_d[I_2] - k_t[R\bullet]^2, \text{ decomposition limited} \tag{15a}$$

$$\frac{d[R\bullet]}{dt} = k_i[I\bullet][m] - k_t[R\bullet]^2, \text{ initiation limited} \tag{15b}$$

The QSSA assumes that the rate that $[R\bullet]$ changes at is very slow compared to the other processes (decomposition, initiation, propagation, termination); i.e. it is assumed that $\frac{d[R\bullet]}{dt} \approx 0$.

In this work the initiator decomposes very slowly so that $[I_2] \sim [I_2]_0$, where $[I_2]_0$ is the initial concentration of initiator. Eq. (14) then yields the forms

$$[m] = [m]_0 \exp(-\alpha t), \alpha = k_p[R\bullet] = k_p\sqrt{\frac{2Fk_d}{k_t}},$$

decomposition is rate limiting (16)

If initiation is diffusion controlled (Eq. (12b)) then

$$[m] = \frac{[m]_0}{\left(1+\sqrt{\frac{[m]_0}{4}}\beta t\right)^2}, \qquad \beta = k_p\sqrt{\frac{I\bullet k_i}{k_t}},$$

initiation is diffusion controlled (17)

Recently, this group experimentally monitored and quantified the cross-over from decomposition-controlled initiation (Eq. (12a)) to diffusion-controlled initiation (Eq. (12b)) for free radical polymerization of acrylamide [47]. The QSSA was found to be an excellent basis for describing the cross-over between the regimes, and the expressions (16) and (17) were verified for each case. An important conclusion was that, although the first-order solution (Eq. (16)) is not always rigorously justified, it provided a robust and reasonable fit to the data, even in the case of diffusion controlled initiation. This simplifies computations in what follows, so that Eqs. (12a) and (15a) for decomposition controlled initiation will be used in the formulation of specific semi-batch protocols, but the slightly different results resulting from use of Eqs. (12b) and (15b) for diffusion controlled initiation will be mentioned in some cases.

One of the difficulties of controlling polymerization reactions is the fact that they become highly nonlinear, especially at moderate to elevated reactant concentrations, which change reaction conditions, such as increased viscosity etc. It was recently shown that at low concentrations reactions are "well behaved", kinetic parameters are constant, etc. [47]. This suggests that the reactions are intrinsically linear and the difficulties in the polymerization arise due to high concentrations, exothermicity, heat, mass transfer, etc.

It should be noted that, although no evidence was found for changes in k_p and k_t as a function of conversion for the dilute Am concentrations in this work, there is extensive work on how k_p depends on monomer concentration and conversion [48–51], and how k_t depends on chain length [52,53]. In aqueous polymerization k_p can show different behavior than for non-aqueous solutions [2]. In particular, there has been work devoted to acrylamide [54–56], which also showed that reaction rate coefficients for Am are not constant during the polymerization reaction, at least at relatively high monomer concentrations (>10% monomer by weight in solution). There are theoretical explanations [57–59] for the changing rate coefficients. These models have been experimentally verified only at high concentrations. Seabrook et al. report [60], however, that k_p and k_t do not change during reactions at lower monomer concentrations (below 10% monomer by weight), consistent with this group's measurements.

The molecular weight approach of the predictive control approach can be addressed using the kinetic chain length concept for free radical polymerization; the instantaneous number average chain length $N_{n,inst}$ ($N_{n,inst}$ is the number of units in the chain) is given by

$$N_{n,inst} = \frac{k_p[m]}{Yk_t[R\bullet] + k_3[S]} \tag{18}$$

where k_3 is the rate constant for chain transfer from propagating radical to chain transfer agent of concentration $[S]$, and Y is a factor which is equal to 1 when recombination dominates, and 2 when disproportionation dominates, and takes on values between these limits when both termination mechanisms are present. In this work with Am there is no measurable chain transfer so that k_3 is taken as zero in subsequent computations.

2.3. Computing polymer concentration and monomer conversion

Now it is of interest to consider the monomer and polymer mass balance in the reactor, which will allow monomer conversion to be defined, and to permit computation of M_w and $[\eta]_w$ from light scattering, viscosity, and concentration data. These computations require knowledge of the polymer concentration, yet one normally directly measures the monomer concentration. Polymer concentration is then found by mass balance.

Let $m_c(t)$ be the cumulative (or total) mass of monomer plus polymer in the reactor, which is the sum of initial monomer mass in the reactor m_0 and that flowed in from the external reservoir, minus the amount flowed out for ACOMP sampling. This is computed by solving

$$\frac{dm_c(t)}{dt} = c_m' Q_m(t) - q\frac{m_c(t)}{V(t)} \tag{19}$$

For free radical reactions, where there is no elimination and condensation of products, a direct mass balance can be invoked to relate monomer and polymer mass via

$$m_c(t) = m(t) + m_p(t) \tag{20}$$

where $m(t)$ and $m_p(t)$ are the monomer and polymer mass in the reactor, respectively. The ACOMP detector train provides a direct measurement of $m(t)$, typically using the UV absorbance spectra and/or refractive index data. $m_c(t)$ is computed via Eq. (19), whence $m_p(t)$ is directly extracted from Eq. (20), and $c_p(t) = m_p(t)/V(t)$ is computed. Density changes, while measurable, are usually small (and in fact negligible in this work, due to the very low Am concentration), and are not corrected for in this work. They have been addressed in the ACOMP context previously [45,61].

A typical scenario would be flowing monomer into the reactor at a constant rate $Q_m(t) = \rho$ from a monomer reservoir at concentration c_m', with an initial amount of monomer m_0 in the reactor, and a constant, small ACOMP withdrawal stream at rate q. Solving Eq. (19), subject to $m_c(0) = m_0$ yields:

$$m_c(t) = \frac{m_0}{\left(1+\frac{(\rho-q)}{V_0}t\right)^{q/(\rho-q)}} + \rho c_m' t \tag{21}$$

It is also important to have a measure of fractional monomer conversion f in the reactor at any time. The simplest means, in keeping with standard batch parlance, is to

define 'instantaneous conversion' $f(t)$ as the total mass of polymer in the reactor divided by the total mass of combined monomer plus polymer in the reactor ($m_c(t)$)

$$f(t) = \frac{m_c(t) - m(t)}{m_c(t)} \tag{22}$$

Although termed 'instantaneous conversion', it is actually the accumulated state of conversion of all monomer in the reactor at time t.

In terms of reaction completion for a specified process, in which a certain total mass of monomer $m_{c,f}$, is to be converted completely to a corresponding amount of polymer in the reactor, the 'foreseen' conversion f_v (v for 'vorausgesehen') is

$$f_v(t) = \frac{m_{c,f} - m(t)}{m_{c,f}(t)} \tag{23}$$

Eq. (18) gives the instantaneous number average degree of polymerization $N_{n,inst}$. The instantaneous number average molecular weight is simply $M_{n,inst} = N_{n,inst}M_m$, where M_m is the monomer molecular weight. The instantaneous weight average molecular weight $M_{w,inst}$ is related to $M_{n,inst}$ by $M_{w,inst} = wM_{n,inst}$, where w is the 'instantaneous polydispersity', which is typically less than 2 for free radical polymerization. The cumulative weight average molecular weight $M_w(t)$, can be conveniently calculated using the mass of polymer in the reactor $m_p(t)$;

$$M_w(t) = \frac{\int_0^t M_{w,inst}(t)dm_p(t)}{m_p(t)} \tag{24}$$

This can be used for predicting values of $M_w(t)$, which is what the multi-angle light scattering in ACOMP measures directly. On the other hand, it can be valuable to use $M_w(t)$ from ACOMP to compute $M_{w,inst}(t)$ as follows

$$M_{w,inst}(t) = \frac{d(M_w(t)m_p(t))}{dm_p(t)} \tag{25}$$

It is noted that Eqs. (24) and (25) depart from traditional batch ACOMP in that the latter use fractional monomer conversion f, or polymer concentration c_p, instead of $m_p(t)$ as the variable of integration. That works for batch reactions with f because in that case f is a function of only one time dependent variable $c_m(t)$, and $f(t) = 1 - c_m(t)/c_{m,0}$, where $c_{m,0}$ is the starting concentration of monomer in the reactor. $f(t)$ for the semi-batch formalism, Eq. (22), is a function of two time dependent variables and would not properly average M_w if used as the variable of integration.

2.4. A note on concentration notation

For convenience, and in keeping with the central aim of determining masses in the reactor, concentrations in data tables and figures will usually be represented as mass concentrations for solute s as c_s (g/cm^3), whereas reaction rate equations use the molar concentration of s, [s] (mol/L).

2.5. Semi-batch procedures used in this work

Initial exploration of predictive control in this work was done under two situations. (I) Monomer in a reservoir at concentration c_m' was flowed into the reactor with a flow rate $Q_m(t)$. (II) Initiator in a reservoir at concentration c_I' was flowed into the reactor with a flow rate $Q_I(t)$, or, alternatively, added in discrete 'delta-function' injections.

3. Materials and methods

Free radical polymerization of acrylamide (Am) in aqueous solution was chosen to demonstrate the predictive control approach to semi-batch reactions. Acrylamide (99 + %, electrophoresis grade, hereafter Am) and potassium persulfate (99 + % A.C.S. reagent, hereafter KPS) were purchased from Aldrich and used without further purification. Water was deionized and filtered with 0.22 μm filter in a Modulab UF/UV system. Polyacrylamide is denoted as pAm.

All experiments were carried out at 60 °C where $k_d = 1.925 \times 10^{-5}$ s^{-1} for KPS (from Sigma–Aldrich website: http://www.sigmaaldrich.com/img/assets/3900/Thermal_Initiators.pdf); i.e. it is possible to use the approximation that $[I_2](t) \sim [I_2]_0$, since the reaction times were on the order of an hour and $1/k_d = 14.5$ h.

The principle of ACOMP and system specifics have been reported previously in detail [1,2,62]. Am kinetics were studied by ACOMP previously, although the central issue of this work, predictive control of molecular weight, was not explored [63]. The ACOMP system in this work used a two pump, one stage dilution in a high pressure mixing chamber (HPMC), yielding from 11- to 23-fold dilution depending on the amount of monomer concentration. The dilution solvent was aqueous 0.1 M NaCl. A Shimadzu HPLC pump was used for extraction from the reactor at $q = 0.1$ cm^3/min, and an Agilent pump was used to bring the solvent to the HPMC. The total detector flow rate was from 1.1 to 2.26 ml/min, yielding from 0.00013 to 0.0012 g/cm^3, depending on the experiment, of combined monomer and polymer concentration in the detector train. Detectors comprised a Brookhaven Instruments Corporation (BI-MwA) multi-angle light scattering photometer (MALS), a Shimadzu RID-10A differential refractometer (RI), a custom-built single capillary viscometer [64], and a Shimadzu photodiode array SPM-20A UV/visible spectrophotometer (UV).

Another programmable Shimadzu HPLC pump was used to deliver solutes to the reactor in the semi-batch processes. Monomer was delivered to the reactor at constant feeds of 0.2 cm^3/min and 0.48 cm^3/min where the reservoir concentration was 0.16 g/cm^3. Initiator, in one case, was delivered at constant feed of 0.94 cm^3/min. In another case the pump was programmed to increase the feed linearly with the slope of 0.04 cm^3/min^2. An experiment with a series of initiator injections was also performed. The initiator reservoir concentration was 0.042 g/cm^3. In all cases reservoirs were continuously stirred and degassed with nitrogen.

The reactions were conducted in a three neck reactor. One neck was used for a condenser, a second for solute and nitrogen delivery and the third for the extraction from the reactor. The reactor was continuously degassed with nitrogen. In order to keep the reactor temperature constant

it was immersed in an oil bath that was kept at 65 °C. The temperature in the reactor was 60 °C, and monitored by a thermocouple.

Conversion of Am was determined using the decrease in the UV signal at $\lambda = 240$. The data were corrected due to polymer absorption/scattering that was obtained from a semi-batch experiment with a constant inflow of the initiator to the reactor. In that experiment monomer was fully depleted and the small, residual UV absorbance/scattering was due to the polymer. M_w was determined using the usual Zimm equation [65] in the ACOMP context, and weight averaged reduced viscosity, $\eta_{r,w}$, according to previously described ACOMP methods [1]. Under these low concentrations and shear rates ranging from 950 [1/s] to 1950 [1/s] η_r is very close to $[\eta]_w$, which was verified by separate measurements, and so they are taken to be equal in the results, and $[\eta]_w$ is used henceforth.

The highest monomer and polymer concentration reached in the reactor was 0.03 g/ml, since beyond this concentration, under the temperature and initiator conditions used here, there is strong reaction exothermicity and the reactor liquid becomes viscous, leading to the so-called 'Trommsdorf', or 'gel-effect', after which the reaction kinetics no longer resemble the idealized mechanism. It should be noted, however, that ACOMP systems have been developed to continue working at very high reactor viscosities, up to about 10^6 cP [66], and the control approach taken here should be readily usable at much higher reactor concentrations without any problems.

After obtaining detector baselines with the aqueous solvent, the monomer solution was heated up and once the temperature was stable the initiator was added. It was verified that there was no thermal polymerization in the absence of initiator.

The SEC system used an LC-ATvp Shimadzu HPLC pump, with Shodex 804HQ and 806HQ columns in series. The injector loop was 100 μl and a flow rate of 0.8 ml/min was used. The detector train included a Brookhaven Instruments Corporation MALS (BI-MwA), Waters 410 RI, and a custom built capillary viscometer. The eluent was 0.1 M NaCl aqueous solvent.

3.1. Convolution problem: extracting reactor component concentrations using the ACOMP system response function

Because high resolution in the conversion kinetics was sought, the effects of the ACOMP temporal response function were accounted for by deconvolving the UV signal. The signals recorded by ACOMP are convolved according to:

$$D(t) = \int_{-\infty}^{\infty} R(t-\tau)S(\tau)d\tau \tag{26}$$

where $D(t)$ is the detected (measured) signal, $R(t)$ is the response function of the system and $S(t)$ is the true concentration or other physical signal that is to be recovered through deconvolution.

A common approach to the deconvolution problem is via the convolution theorem which states that for two functions f and g, under suitable conditions a Fourier transform of the convolution of f and g, denoted as $f * g$, is a product of Fourier transforms, i.e.:

$$F\{f * g\} = F\{f\} \cdot F\{g\} \tag{27}$$

In principle a signal can be deconvolved by taking the reverse Fourier transform of the ratio of Fourier transforms of the measured (or detected) signal $D(t)$and the response function $R(t)$:

$$D(t) = F^{-1}\left\{\frac{F\{M(t)\}}{F\{R(t)\}}\right\} \tag{28}$$

However, this approach is extremely sensitive to noise and failed to produce good results for the data here. For that reason a Bayesian-based iterative method [67] was implemented, which treats point spread functions as probability-frequency functions and applies Bayes's theorem [68]. Prof. Dimitri Uskov (Tulane University) provided his algorithm adapted to this treatment using the program Mathematica®.

The ACOMP system response function $R(t)$ was determined experimentally by rapidly injecting Am into the reactor to cause a step function in concentration (measured by the UV absorbance in this case):

$$S(t) = \begin{cases} 1 & t \geqslant t_0 \\ 0 & t < t_0 \end{cases} \tag{29}$$

The derivative of the corresponding measured $D(t)$ was used to compute $R(t - t_0)$. t_0 is the lag time between withdrawal of a fluid element from the reactor and its detection, and ranged between 6.5 and 10 min, depending on the flow rate to the detectors. In the limit of instantaneous system response $R(t - t_0)$ becomes the delta function $\delta(t - t_0)$

$$\frac{dD(t)}{dt} = \int_{-t_0}^{\infty} \frac{d}{dt} R(t-\tau)d\tau = R(t-t_0) \tag{30}$$

The deconvolved concentration signals are shown and analyzed in the Results section. They are not much different than the undeconvolved data, but provide sharper initial data which helps in the precision of the predictions.

3.2. Assessment of detection for flowing components, without reactions

In the batch situation above, where the only flow is the ACOMP extraction flow rate q, the detector train furnishes all information concerning conversion of monomer mass into polymer, without any auxiliary information. Unlike the no-flow situation, the semi-batch operation requires that flow conditions into and out of the reactor be separately known in order to interpret the detector signals in terms of monomer conversion into polymer and carry out the associated M_w and $[\eta]_w$ calculations.

The purpose of this section is to verify the accuracy of the flow feeds and withdrawals and their effect on the reactor contents and detector signals when no reaction occurs. The general form for $m_s(t)$ when no reactions occur is Eq. (1) with ε_s and $\gamma_s(t)$ both zero. The solution will depend on the forms of $Q_s(t)$ and $V(t)$.

3.3. The case where liquid flowing into reactor does not contain component s

This corresponds to the case where there is ACOMP extraction at rate q and a flow of some other component x (or just solvent) into the reactor $Q_x(t)$, but no flow of component s into the reactor. In the case where no reactions are taking place, it is simpler to use the mass equations rather than concentration equations, so that

$$m_s(t) = m_{s,0} \exp\left\{-q \int_0^t \frac{dt'}{V(t')}\right\} \tag{31}$$

and then $c_s(t)=m_s(t)/V(t)$.

3.3.1. Constant flow rate into reactor at ρ (cm^3/s) of component x (e.g. pure solvent)

With $Q_x(t) = \rho$, where ρ = constant, and the usual ACOMP extraction flow rate of q, $V(t) = V_0 + (\rho - q)t$. Then, performing the integral in Eq. (31) above and division by $V(t)$ yields the following temporal dilution profile for the mass concentration of any component s, present in the reactor at initial concentration $c_{s,0}$

$$c_s(t) = \frac{c_{s,0}}{\left(1 + \frac{\rho - q}{V_0} t\right)^{\rho/(\rho - q)}} \tag{32}$$

Fig. 1 shows the predicted result for $c_{Am}(t)$ (dashed line, not a fit), and the experimentally measured result (solid black curve) for an experiment in which pure water was flowed into the reactor containing an initial amount of Am, under the following conditions: $c_{Am,0} = 0.0153$ g/cm^3, $V_0 = 49.93$ cm^3, $\rho = 1.8$ cm^3/min, and the constant ACOMP extraction rate was $q = 0.001667$ cm^3/min. The agreement is excellent in this case, and allows the analytical expression for concentration to be used in predictive control applications.

3.3.2. The addition rate of component x increases linearly with time, $Q_x(t) = \sigma t$

With $Q_x(t) = \sigma t$, where σ = constant, and the usual ACOMP extraction flow rate of q, $V(t) = V_0 - qt + \sigma t^2/2$. Performing the integral in Eq. (31) yields

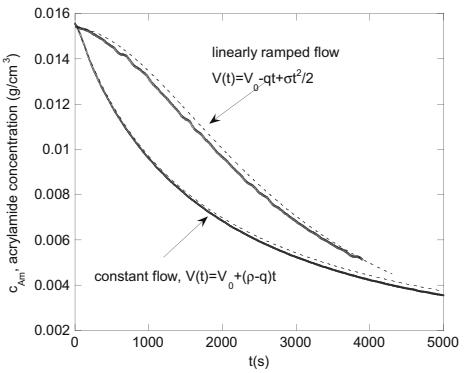

Fig. 1. Effect of pure solvent flow into reactor on c_{Am} when no reaction is occurring for (i) constant flow rate into reactor $Q_x = \rho$ and (ii) a linearly ramped flow $Q_x(t) = \sigma t$. Dashed lines are computations (not fits) according to Eqs. (32) and (33).

$$c_s(t) = \frac{c_{s,0} \exp\left\{-\frac{2q}{\sqrt{2\sigma V_0 - q^2}} \tan^{-1}\left(\frac{-q + \sigma t}{\sqrt{2\sigma V_0 - q^2}}\right)\right\}}{\left(1 - qt + \frac{\sigma}{2V_0} t^2\right)} \tag{33}$$

Fig. 1 also shows the predicted (dashed line, not a fit) and measured concentrations of Am, using the above profile under the following conditions: $c_{Am} = 0.0154$ g/cm^3. ACOMP extraction rate was $q = 0.001667$ cm^3/s, initial reactor liquid volume $V_0 = 48.1$ cm^3, and the positively tapered flow rate was $\sigma = 0.2$ cm^3/min^2 $= 5.56 \times 10^{-6}$ cm^3/s^2. The result again agrees well with the prediction.

4. Results

Table 1 gives a summary of the various reactions described below, including the conditions used, reactant feed rate, etc.

4.1. Pure batch reaction, no flow into the reactor (#1)

A pure batch Am reaction was performed to provide the basic rate coefficient on which to base subsequent predictions. As derived above, the pure batch equations apply if the only flow during the experiment is the ACOMP extraction flow rate q, from the reactor. Monomer concentration for a batch experiment in CGS units is given by:

$$c_m = c_{m,0} \exp(-\alpha t), \qquad \alpha = k_p[R\bullet] \tag{34}$$

As shown in Ref. [51] at such a low monomer concentration monomer diffusion affects the rate of polymerization, so that an exponential fit is not rigorously valid, and is, in fact, measurably worse than a fit according to Eq. (17). Nonetheless, the exponential fits representing decomposition limited initiation are robust enough to make useful predictive calculations. For experiment #1 an exponential rate coefficient $\alpha = 0.00056$ [1/s] was found. This value is used in subsequent analysis and predictive control. Run-to-run reproducibility of α under nominally identical reaction conditions was ±5%.

Fig. 2 shows M_w and $[\eta]_w$ vs. f for the batch experiment (#1). Over the first 20% of conversion M_w and $[\eta]_w$ are far above the QSSA prediction, which for M_w is a straight line; $M_w(f) = M_{w,0}(1 - f/2)$, where f is fractional monomer conversion. The trend of M_w reaches the QSSA condition after $f = 0.2$. The QSSA prediction that $M_w(f = 1) = 0.5M_w(f = 0)$, is closely met by the fit shown over the linear regime.

4.1.1. Monomer is fed into the reactor at $Q_m(t)$

A powerful means of controlling M_w is to feed monomer into the reactor at a rate $Q_m(t)$ from a reservoir of monomer concentration c_m'. Following the above procedure for taking into account both the decomposition reaction ($d[I_2]/dt = -k_d[I_2]$) and the inflow and outflow, the molar initiator concentration in the reactor is

$$\frac{d[I_2]}{dt} = -[I_2]\left(k_d + \frac{Q_m(t)}{V(t)}\right) \tag{35}$$

Likewise, the molar monomer concentration in the reactor is,

Table 1
Summary of reactions. All were carried out at $T = 60$ °C, $q = 0.001667$ cm^3/s for all experiments.

Expt. #	Exp description	c_{Am} ($t = 0$) [g/cm^3]	Initiator ($t = 0$) [g/cm^3]	c_s' [g/cm^3]	V_0 [cm^3]	Q_s [cm^3/min]	σ [cm^3/min^2]	$M_{w,\text{final}}$ (g/mol)	$[\eta]_w$ [cm^3/g]
1	Batch	0.005	0.00078	N/A	199.9	N/A	N/A	80,000	30
2	Am flow to keep M_w const	0.005	0.00078	0.156	222	0.2	N/A	260,000	120
3	Am flow to increase M_w	0.003*	0.00047	0.156	192	0.48	N/A	700,000	180
4	Constant KPS flow	0.005	0.00000	0.043	99.2	0.94	N/A	60,000	20
5	Linearly increasing KPS flow	0.005	0.00000	0.042	200.1	N/A	0.08	70,000	30
6	Initiator delta injections*	0.005	0.00011	N/A	198.7	N/A	N/A	80,000	40

* Final $c_{Am} = 0.0089$ g/cm^3.

$$\frac{d[m]}{dt} = -[m]\left(k_p[R\bullet] + \frac{Q_m(t)}{V(t)}\right) + \frac{[m]'Q_m(t)}{V(t)} \tag{36}$$

where $[m]' = c_m'/v_m$ is the molar monomer concentration in the monomer reservoir feeding the reactor. The expression used for $[R\bullet]$ depends on whether initiation is decomposition controlled (Eq. (12a)) or diffusion controlled (Eq. (12b)). It will generally be assumed that initiation is decomposition controlled. Once this equation is solved for $[m]$ the polymer mass in the reactor can be solved from mass balance.

Although the procedure only involves first-order differential equations, the solutions can nonetheless be quite complex for arbitrary forms of $Q_m(t)$ and magnitudes of q and $Q_s(t)$. Of course, the solutions can always be found numerically, so that the method is computationally robust.

4.1.1.1. Constant flow rate of monomer into the reactor $Q_m = \rho$ (cm^3/s) = constant. The solution to Eq. (35) with constant monomer flow into the reactor, $Q_m(t) = \rho$ can be found by direct integration to be

$$[I_2] = \frac{[I_2]_0 e^{-k_d t}}{\left(1 + \frac{(\rho - q)}{V_0}t\right)^{\rho/(\rho - q)}} \tag{37}$$

Eq. (15a) can be used to determine $[R\bullet] \approx \sqrt{2Fk_d[I_2](t)/k_t}$ within the QSSA. Using $[I_2]$ from Eq. (37) for $[I_2](t)$ can be substituted into Eq. (36), and the resulting integral solved numerically. There are two good approximations that can be made, however, in order to obtain a good analytical solution. First, [Am]′ in the feed reservoir can be made high enough that only a low flow rate Q_m is needed so that relatively little increase of V_0 occurs during the reaction (<10%). Then $V(t) \approx V_0$. Furthermore, as mentioned above, the half life of KPS at 60 °C is long compared to the reaction, so the approximation can be used that $[I_2](t) \approx [I_2]_0$. With this, the molar monomer concentration is calculated to be

$$[m](t) = [m]_0 \exp\left\{-\left(\frac{\rho + \alpha V_0}{V_0}\right)t\right\} + \left(\frac{[m]'\rho}{\rho + \alpha V_0}\right)\left(1 - \exp\left\{-\left(\frac{\rho + \alpha V_0}{V_0}\right)t\right\}\right) \tag{38}$$

Eq. (38) has several interesting features. First, it predicts that the rate coefficient controlling monomer concentration increases from α to $\alpha + \rho/V_0$, where the added term reflects the result of the added volume diluting the reactor. For the conditions in Table 1, this dilution amounts to only about a 10% increase over the reaction rate coefficient (α) for each of the two experiments shown. Second, the concentration of monomer in the reactor, in this approximation, approaches a steady state value, $[m]_{ss}$, given by

$$[m]_{ss} = \left(\frac{[m]'\rho}{\rho + \alpha V_0}\right) \tag{39}$$

This value is approached with the same rate coefficient $\alpha + \rho/V_0$, and this steady state concentration may be greater than, less than, or equal to $[m]_0$. In fact these three regimes provide a convenient labeling for the period during which the steady state is being approached:

$$(i)\left(\frac{[m]'\rho}{\rho + \alpha V_0}\right) < [m]_0 \quad \text{'Starved regime'} \tag{40a}$$

$$(ii)\left(\frac{[m]'\rho}{\rho + \alpha V_0}\right) > [m]_0 \quad \text{'Flooded regime'} \tag{40b}$$

$$(iii)\left(\frac{[m]'\rho}{\rho + \alpha V_0}\right) = [m]_0 \quad \text{'Isoreactive regime'} \tag{40c}$$

The terms 'starved regime' and 'flooded regime' are in common parlance for semi-batch reaction work, especially as regards emulsion polymerization [69]. The starved regime means that all monomer flowing into the reactor is being consumed in addition to the remaining $[m]_0$, whereas in the flooded condition, the inflow of monomer is fast enough that it cannot all be consumed together with the remaining $[m]_0$, so that monomer concentration builds up in the reactor.

In the isoreactive regime the rate of monomer addition is just enough to offset the rate of monomer conversion to polymer, and to keep the concentration in the reactor constant. This condition also leads to a constant instantaneous molecular weight, by Eq. (18), as long as $[R\bullet]$ remains approximately constant because of slow initiator decomposition.

The existence of the different approach regimes suggests that an index comparing the rates of change of $[m]$ due to the polymerization reaction and, separately, due to the flow, would be useful. With this the 'Approach Index' can be defined as

$$A = \frac{(dm/dt)_{\text{reaction}}}{(dm/dt)_{\text{flow}}} \tag{41}$$

Some authors occasionally refer to this or a similar quantity as 'instantaneous conversion'. Since A can be greater than unity in Eq. (41) definition it does not resemble a usual fractional monomer conversion, such as in a

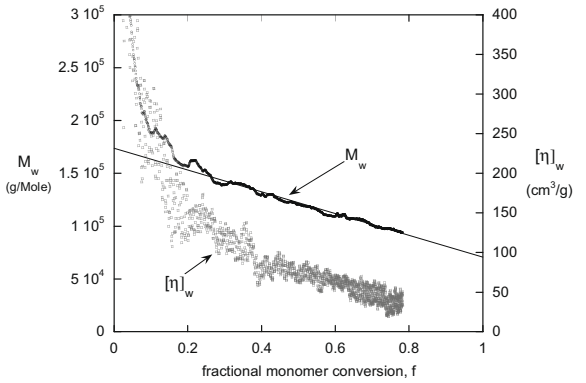

Fig. 2. M_w and $[\eta]_w$ vs. f (fractional monomer conversion) for batch free radical polymerization of Am (experiment #1).

batch situation, so the 'Approach Index' term is used. For the type of reaction here, and under the scenario of flowing in monomer, A becomes

$$A = \frac{\alpha[m](t)V(t)v_m}{c'_m Q_m(t) - \frac{qm(t)}{V(t)}} \tag{42}$$

Fig. 3 shows the computed 'instantaneous' conversion f_c, and the Approach Index A, for experiments #2 (Isoreactive) and #3 (Flooded). Also shown are f_c and A for a hypothetical starved case, in which $c_{Am,0} = 0.005$ g/cm^3, $\rho = 0.00333$ cm^3/s, $V_0 = 200$ cm^3, $c'_{Am} = 0.054$ g/cm^3, and $\alpha = 5.2 \times 10^{-4}$ s. The steady state value of A at high conversion is $A \approx \alpha V_0/(\rho + \alpha V_0) < 1$. This is less than unity at the steady state because in order for $[m]$ to remain constant at steady state the amount of monomer flowed into the reactor per second must compensate both the reaction that consumes monomer and the dilution of the reactor contents caused by the flow itself.

4.1.1.2. Keeping M_w constant during the reaction, the 'Isoreactive regime'. According to Eq. (18), keeping $[m]$ constant while $[R\bullet]$ remains constant should lead to a constant, non-drifting molecular mass. Hence, an attempt was made to keep monomer concentration constant during the reaction. The necessary monomer inflow to keep $[m]$ constant is (Eq. (40c))

$$\rho = \frac{\alpha V_0 [m]_0}{[m'] - [m]_0} \tag{43}$$

Experiment #2, with $c_{Am,0} = 0.005$ g/cm^3 ($[m]_0 = 0.071$ mol/L) was carried out under this condition.

Fig. 4a shows that the monomer concentration stayed constant during the experiment and the polymer concentration changed linearly as predicted by Eq. (44) when ρ = constant and $[m](t) = [m]_0$ = constant, and $V(t) \approx V_0$,

$$c_p(t) \approx \frac{\rho c'_m}{V_0} t \tag{44}$$

when $[m](t)$ = constant, and $[R\bullet] \cong$ constant, as in this work, the cumulative weight average molecular weight equals the instantaneous weight average molecular weight,

$$M_w = M_{w,inst} = \frac{wM_{Am}k_p[m]_0}{k_t[R\bullet]} = 1000wc_{m,0}\frac{k_p^2}{\alpha k_t} \tag{45}$$

where w is the instantaneous polydispersity M_w/M_n. The following parameters were used to compute M_w: $k_p^2/k_t = 14.7$ (L/M s), (where $w = 2$ was used in reference 63), $\alpha = 0.00052$ s^{-1} (from the batch experiment #1, above), $c_{m,0} = 0.005$ g/ml. The computation yielded: $M_w = 262{,}500$ which is in excellent agreement with experiment #2.

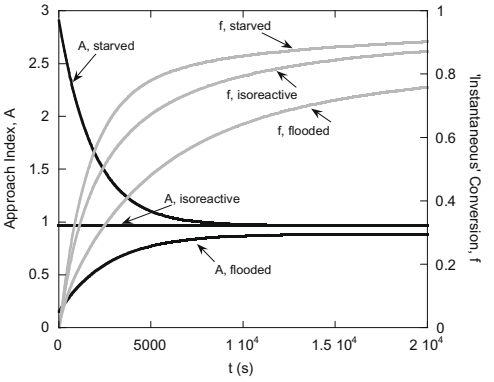

Fig. 3. Computations of approach index A, and 'instantaneous' conversion, for semi-batch reactions in the isoreactive (#2), flooded (#3), and starved (hypothetical $\rho = 0.003$ cm^3/s, $V_0 = 200$ cm^3 $c_{m,0} = 0.005$ g/cm^3, and $c_m' = 0.052$ g/cm^3). Also shown are the cumulative monomer conversion functions f_c.

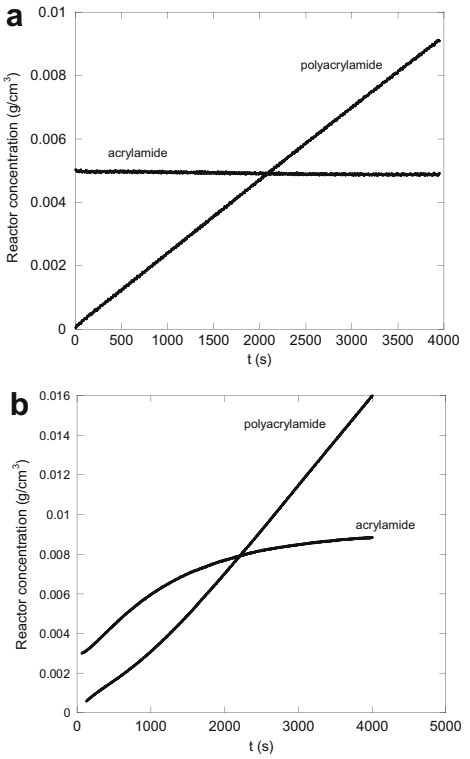

Fig. 4. (a) c_{Am} and c_{pAm} (polymer concentration) for experiment #2, where M_w was kept constant. (b) c_{Am} and c_{pAm} for experiment #3, where M_w was made to increase during conversion.

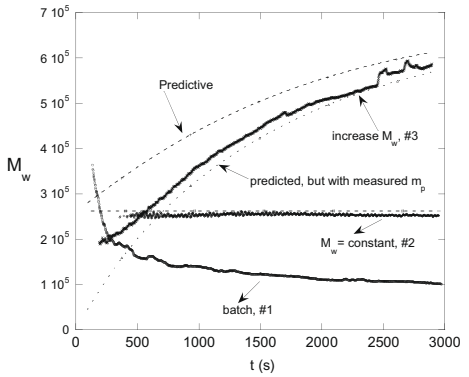

Fig. 5. M_w vs. time for semi-batch experiment #2, where M_w was held constant, and #3, where M_w was increased in a predicted fashion. The dashed lines near the curves for experiments #2 and #3 (Eq. (47)) are the predictions (not fits). See text for origin of second dashed line 'predictive but with measured m_p'. For reference, the pure batch experiment, #1, is also shown.

Fig. 4b shows monomer and polymer concentration in the reactor for the flooded regime, and is described below.

Fig. 5 shows the results for M_w vs. t for experiment #2, where $[m]$ was held constant, along with the dashed line prediction. The experiment was successful in keeping M_w constant. As a reminder, the curve below that for experiment #2 is the batch result (#1), which decreases vs. t without semi-batch intervention. Fig. 6 shows $[\eta]_w$ for experiment #2, where $[m]$ was held constant. This is also contrasted with $[\eta]_w$, the batch experiment (#1), for which $[\eta]_w$ decreases vs. t.

4.1.1.3. Increasing M_w during the reaction. The adjustable feed rate confers great power for controlling M_w during the reaction. Whereas the last experiment showed how M_w can be kept constant, and no feed at all (pure batch) leads to decreasing M_w during the reaction, Eqs. (18) and (38) suggest that it can also be made to increase in a predictable fashion during the experiment. This requires a higher value of the monomer flow rate ρ and operation in the 'flooded' regime defined by Eq. (40b). For this situation, using Eqs. (20), (21), and (38), yields for $c_p(t)$

$$c_p(t) = \frac{m_0 + \rho c'_m t}{V(t)} - [m]_0 \exp\left(-\frac{\rho + \alpha V_0}{V_0} t\right) - \frac{[m]'\rho}{\rho + \alpha V_0}\left\{1 - \exp\left(-\frac{\rho + \alpha V_0}{V_0} t\right)\right\} \quad (46)$$

and M_w is computed by Eq. (25) to be

$$M_w = \frac{2000\,\frac{k_p^2}{k_t}}{\alpha}\frac{1}{V_0 + \rho t} \times \left(\frac{\frac{2}{\alpha}(\rho c'_m m_0 - \frac{\rho^2 c'^2_m}{\alpha})(1 - e^{-\alpha t})}{\rho c'_m t + m_0 - (m_0 - \frac{\rho c'_m}{\alpha})e^{-\alpha t} - \frac{\rho c'_m}{\alpha}} + \frac{\frac{1}{2\alpha}(\alpha m_0^2 - 2\rho c'_m m_0)(1 - e^{-2\alpha t})}{\rho c'_m t + m_0 - (m_0 - \frac{\rho c'_m}{\alpha})e^{-\alpha t} - \frac{\rho c'_m}{\alpha}} + \frac{\frac{\rho^2 c'^2_m}{\alpha} t}{\rho c'_m t + m_0 - (m_0 - \frac{\rho c'_m}{\alpha})e^{-\alpha t} - \frac{c'_m}{\alpha}} \right) \quad (47)$$

The predicted M_w was computed using the following parameters: $\frac{k_p^2}{k_t} = 14.7$ (L/M s), $\rho = 0.008$ cm^3/s, $c'_m = 0.160$ [g/cm^3], $m_0 = 0.562$ g. α was obtained by taking α from experiment #1 ($\alpha = 0.00056$ s^{-1}) and correcting it with appropriate initiator and monomer concentrations according to $\alpha = \alpha_{\#1}\sqrt{\frac{c_I c_m}{c_{I,\#1} c_{m,\#1}}} = 0.00033$ s^{-1}. The predicted (according to Eq. (47)) and experimental M_w are shown in Fig. 5. The prediction is in fair agreement with the experiment, but is not as precise as the predicted trend for #3. It is important to point out that small deviations in the integral numerator of Eq. (24) and the denominator can lead to substantial errors, especially at early conversion, where these quantities are small. The dashed line labeled 'Predictive but with measured m_p' is the computation of M_w using the online *measured*, rather than predicted m_p (the other dashed line). The result is clearly better, and illustrates how input concentrations from monitoring can be superior predictors of M_w than the purely predictive ones.

4.1.1.4. SEC results for M_w control experiments. Fig. 7 shows the MWD obtained from the multi-detector SEC instrumentation, and Table 2 gives the numerical results of the corresponding analyses. The MWD show how effective the program of maintaining constant M_w was, since its width is significantly less than the other two experiments, pure batch (#1), and increasing M_w (#3). In fact, the widths for reactions #2 and #3 are less than what would normally be expected in free radical polymerization. The elution in

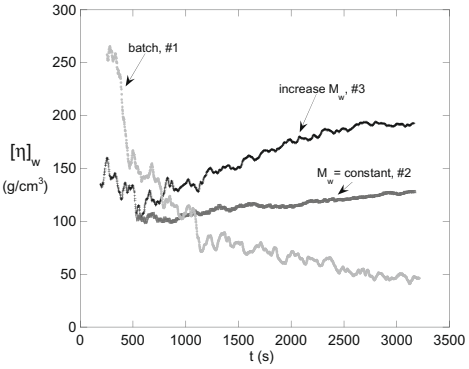

Fig. 6. $[\eta]_w$ vs. time for semi-batch experiment #2, where $[\eta]_w$ was held constant, and #3, where $[\eta]_w$ was increased. For reference, $[\eta]_w$ for the pure batch experiment, #1, is also shown.

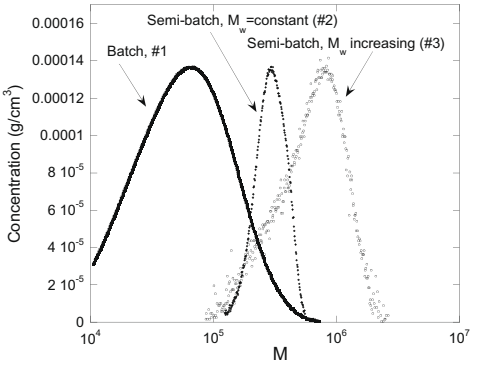

Fig. 7. MWD from multi-detector SEC for experiments #1–#3. The width of the constant M_w semi-batch experiment (#2) is markedly narrower than for the other two experiments, where M_w drifts in time.

Table 2
Multi-detector SEC results for experiments controlling M_w, and the batch experiment. The numbering of the experiments is the same as Table 1.

Expt. #	M_n	M_w	M_z	M at peak	M_z/M_w	M_w/M_n	$[\eta]_w$	M_η*
1	46,000	91,000	167,000	74,000	1.83	1.98	72	66,000
2	246,000	345,000	449,000	290,000	1.30	1.40	142	311,000
3	482,000	713,000	985,000	876,000	1.38	1.49	621	633,000

* M_η = viscosity average mass, computed by $M_\eta = (243.9[\eta]_w)^{1.235}$ (from Ref. [71]).

each case does not fall within the exclusion limit of the column, so the values should be reliable. It is noted that there is no contradiction with the assumption that the width $w = 2$ above, since it is the numerical value of the entire cluster $w\frac{k_p^2}{k_t}$ that is taken from Ref. [63], so any shift downwards in w will result in a corresponding shift upwards for ${k_p}^2/k_t$. There is no obvious explanation as to why the polydispersity indices for experiments #2 and #3 are less than the usual statistical prediction (M_z:M_w:M_n = 3:2:1).

4.1.2. A free radical initiator in a reservoir at concentration c_I' is flowed into the reactor at $Q_I(t)$

In this case the flowing initiator will change both the conversion kinetics and the molecular weight, but offers less straightforward means for controlling molecular weight.

Following the above procedure the concentration of initiator is

$$\frac{d[I_2]}{dt} = -[I_2]\left(k_d + \frac{Q_I(t)}{V(t)}\right) + \frac{[I_2]'Q_I(t)}{V(t)} \tag{48}$$

$[I_2](t)$ is obtained by the above procedure, whence $R\bullet$ can be determined by either Eq. (15a), (15b). Monomer concentration $[m]$ can be computed by

$$\frac{d[m]}{dt} = -[m]\left(k_p[R\bullet] + \frac{Q_I(t)}{V(t)}\right) \tag{49}$$

4.1.2.1. Constant initiator flow, $Q_I(t) = \rho$ = constant. The conditions of the experiments (Table 1) again allow for useful simplifications yielding analytical insight. The loss of reactor fluid due to extraction does not change V_0 significantly over the course of the reaction. Likewise, $Q_s(t)$ does not have to be large in order to create large changes in $[I_2]$ if the reservoir concentration c_I' is large. Considering the inflow of I_2 to be the sole significant source of changing $[I_2]$ (i.e. decomposition is also very slow compared to the inflow), solving for $[I_2](t)$ from Eq. (48) yields

$$[I_2](t) = \frac{[I_2]'\rho}{k_d V_0 + \rho}\left\{1 - \exp\left[-\left(k_d + \frac{\rho}{V_0}\right)t\right]\right\} + [I_2]_0 \exp\left[-\left(k_d + \frac{\rho}{V_0}\right)t\right] \tag{50}$$

For typical experiments (e.g. #3) $\left(k_d + \frac{\rho}{V_0}\right)t_{\max} \sim 0.1$, so that the approximation $e^{-x} \sim 1 - x$ yields

$$[I_2](t) = \frac{[I_2]'\rho}{V_0}t + [I_2]_0\left[1 - \left(k_d + \frac{\rho}{V_0}\right)t\right] \tag{51}$$

(Because the first term quickly becomes larger than the second term, the time dependent term in brackets can also be dropped to a good approximation.)

Using Eq. (49) in the decomposition controlled initiation yields $[m](t)$ to the same level of approximation

$$[m](t) = [m]_0 \exp\left\{-\frac{\rho}{V_0}t - \frac{2\alpha}{3\chi}\left[(\chi t + [I_2]_0)^{3/2} - [I_2]_0^{3/2}\right]\right\} \tag{52a}$$

where

$$\chi = \frac{[I_2']\rho}{V_0} - [I_2]_0\left(k_d + \frac{\rho}{V_0}\right) \tag{52b}$$

(α as defined in Eq. (34)).

When the volume change due to constant initiator flow cannot be ignored, such as in experiment #4 and $Q_I(t)/V(t) \gg k_d$, as it is in the experiments here, solving Eq. (49) using Mathematica® (version 6.0.0) yields:

$$[m](t) = \frac{1}{V_0 + \rho t}\left\{[m]_0 V_0 \exp\left(-\frac{2}{3}k_p t\sqrt{\frac{2Fk_d[I_2]'\rho}{k_t}}\frac{t}{V_0 + \rho t}\right) \times \sqrt{1 + \frac{\rho t}{V_0}}\ \text{Hypergeometric}\,2F1\left(1.5, 0.5, 2.5, -\frac{\rho t}{V_0}\right)\right\} \tag{53}$$

The class of hypergeometric function designated as Hypergeometric2F1 in Eq. (53) is built into Mathematica® and was evaluated for the gray curve shown in Fig. 8, which shows $[m](t)$ for experiment #4 and the prediction according to Eq. (53) (not a fit) in gray scale. The prediction is in fair agreement with the experiment in this case. The prediction using diffusion control of initiation was essentially equivalent to that from decomposition controlled initiation. The result is so close to that for decomposition controlled initiation that it is not shown in Fig. 8.

It is also worth mentioning that if Eq. (52a) is used to fit the data instead of computing the expected data by Eq. (53), the fit to Eq. (52a) is worse than the prediction by Eq. (53), but still qualitatively correct (fit not shown). In that case, the rate coefficients predicted under each type of fit correspond well to the measured value; 0.0000350 $s^{-1.5}$ predicted, 0.0000344 $s^{-1.5}$ measured for decomposition controlled initiation, and 0.000097 $s^{-1.5}$ predicted, 0.000101 $s^{-1.5}$ measured for diffusion controlled initiation.

In terms of the M_w prediction in the decomposition regime yields:

$$M_w = \frac{wM_{mon}k_p[m]_0}{k_t[R\bullet(t)]}\left(1 - \frac{f}{2}\right) = \frac{wM_{mon}\frac{k_p^2}{k_t}}{k_p[R\bullet(t)]}\frac{1000c_{m,0}}{M_{mon}}\left(1 - \frac{f}{2}\right) = \frac{1000w\frac{k_p^2}{k_t}c_{m,0}}{\alpha}\left(1 - \frac{f}{2}\right) \tag{54}$$

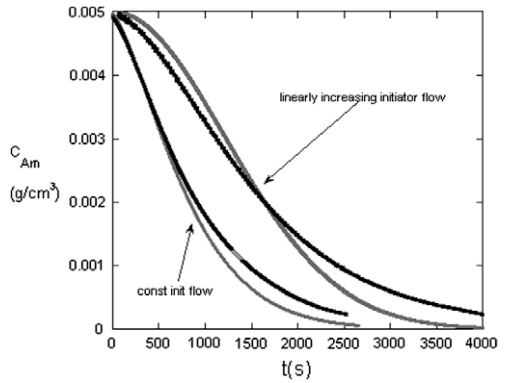

Fig. 8. $c_{Am}(t)$ for reaction #4, in which initiator was flowed into the reactor at constant rate. The calculated curve (not a fit), shown in gray, is from Eq. (53), not a fit. Also shown is $c_{Am}(t)$ for reaction #5, where the initiator flows in at a linearly increasing rate, along with the calculated curve in gray, from Eq. (57).

and in the diffusion regime:

$$M_w = \frac{wM_{mon}k_p[m]_0}{k_t[R\bullet(t)]}\frac{2}{3}\frac{\left(1-(1-f)^{\frac{3}{2}}\right)}{f} = \frac{1000w\frac{k_p^2}{k_t}c_{m,0}}{\alpha}\frac{2}{3}\frac{\left(1-(1-f)^{\frac{3}{2}}\right)}{f} \quad (55)$$

M_w was computed from the above equations again using $\frac{k_p^2}{k_t} = 14.7(\frac{L}{M\times s})$ and $w = 2$, following Ref. [63], $c_{m,0} = 0.005\frac{g}{ml}$ and modifying α based on the batch equation according to the initiator concentration; $\alpha_j = \alpha(\#1)\sqrt{\frac{c_{I,j}}{c_{I}(\#1)}}$. It is noted that since no monomer is fed into the reactor one can use a batch type fractional monomer conversion f, using monomer mass m; $f = 1 - m/m_0$.

The predicted results for both the decomposition and diffusion controlled initiation cases match the measured M_w well, with the diffusion controlled results slightly better. Fig. 9 shows the experimental result and the predicted M_w for the diffusion case (not a fit).

4.1.2.2. Linearly increasing initiator flow, $Q_s(t) = \sigma t$. In this case there was initially no initiator in the reactor; i.e. $[I_2]_0 = 0$. Ignoring the small dilution effect of flowing concentrated initiator into the reactor, and using the fact that the initiator decay is very slow yields, by Eq. (48)

$$[I_2](t) \cong \frac{\sigma[I_2]'t^2}{2V_0} \quad (56)$$

Similarly as in the above example decomposition and diffusion regimes were investigated, but no significant difference was found in the prediction of $c_{Am}(t)$ or $M_w(t)$, so only the decomposition controlled result is presented. In the decomposition case, using Eq. (56) in Eq. (15a) for $[R\bullet]$, then solving the rate equation, a Gaussian conversion profile is obtained:

$$[m](t) = [m]_0 e^{-\frac{k_p}{2}\sqrt{\frac{Fk_d\sigma[I']}{k_t V_0}}t^2} \quad (57)$$

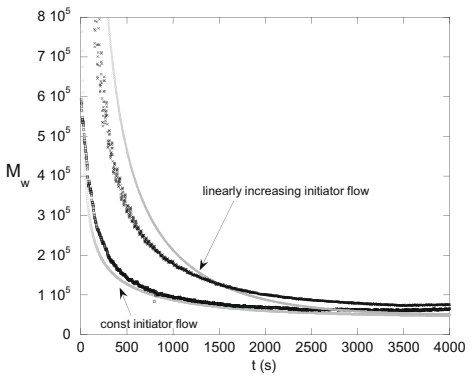

Fig. 9. M_w vs. t for experiments #4 and #5, together with the computed predictions (in gray scale).

where the predicted rate coefficient is $\frac{k_p}{2}\sqrt{\frac{2Fk_d\sigma[I]'}{k_tV_0}} = \frac{\alpha_{\#1}}{2}\sqrt{\frac{\sigma c_I^i}{c_{I,\#1}V_0}} = 3.4\times10^{-7}\ s^{-2}$.

Fig. 8 shows the experimental $c_{Am}(t)$ and the computation in gray scale. The computation is only a fair match to the experimental data, and the deviations are from two sources. First, the prediction does not make provision for residual UV absorbance/scattering, and so declines to zero, whereas a small tail is left in the experimental $c_{Am}(t)$. Secondly, if the experimental $c_{Am}(t)$ is fit with Eq. (57) the fit is excellent, but a rate of $2.03\times10^{-7}\ s^{-2}$ is found, only in fair agreement with the prediction.

M_w was calculated in the same way as in the previous example using the same method for correcting $k_p[R\bullet]$. Fig. 9 depicts the experimental result and the calculated one. These are in fair agreement, with most of the discrepancy coming from the difference between the predicted concentration and the measured one.

4.1.2.3. Delta function initiator addition. Often times in industrial situations initiator is added in 'booster shots' in order to drive a reaction to the highest possible conversion and to 'scavenge' monomer. In this case it is expected that there should be an abrupt increase in the downward

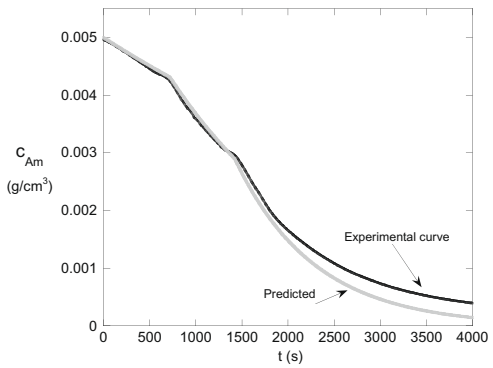

Fig. 10. c_{Am} in the reactor vs. t when two initiator boosts are made after the reaction begins (#6). The gray scale curve is the predicted reaction trajectory (not a fit).

Table 3
Initiator boost experiment #6.

Mon. conc. (g/cm^3)	Initiator conc. (g/cm^3)	Addition time (s)	c_{KPS} (g/cm^3)	Experimental rates (1/s)	Predicted rates (1/s)
0.005	0.000105568	0	0.00011	0.00023	0.000206
0.0043	0.000931407	750	0.00093	0.00056	0.000567
0.0027	0.006222161	1720	0.00622	0.00113	0.00116

slope of $[m](t)$, and an actual discontinuity in $M_{w,inst}(t)$, since the denominator of Eq. (18) (kinetic chain length) abruptly changes. Such a discontinuity in $M_{w,inst}(f)$ has been previously observed by ACOMP monitoring [70].

Fig. 10 shows an example of a reaction where two initiator boosts were given, and Table 3 shows the schedule of initiator booster shots. The gray scale curve in Fig. 10 shows the predicted reaction kinetics using decomposition controlled initiation. Table 3 also shows the predicted and experimentally found rates, which are all quite close to each other.

Again using $\alpha = \alpha_{\#1}\sqrt{\frac{c_I c_m}{c_{I,\#1} c_{m,\#1}}}$ yields the following predicted first-order rate coefficient for the first, second, and third regimes, respectively; 0.000206, 0.000567, and 0.00116 s^{-1}. Fig. 11 shows experimental M_w vs. t for the initiator boosts, as well as the predicted values.

5. Conclusions and outlook

It has been demonstrated that fair to good predictive control of polymer molecular weight and conversion kinetics in semi-batch reactions can be achieved using easily calculable reactor feed rates and reagent reservoir concentrations, and can be verified in near-real time by online monitoring of the reactions. In the case of acrylamide, the QSSA provides a robust analytical framework for computing the reactive part of the reagent balance equations. It was thus demonstrated that M_w during a semi-batch reaction can be held constant or made to increase (or decrease) in predictable fashion, once the underlying batch kinetics are quantified. Many other types of desired profiles for M_w should be attainable by predictive control.

It is recognized, however, that there is room for improvement between the predictions and the results, and that, under stochastic operating scenarios there can be potentially large deviations from the predictions, especially due to unforeseen events. The ability to monitor reactions online, however, will ultimately allow much more precise, active control of the reactions via feedback. Hence, the predictive approach may be ultimately more suited to providing an Ansatz for the reaction protocol, and incremental feedback-controlled adjustments to reactor feed and other conditions can be made automatically via the monitoring signals to keep the reaction headed towards producing the desired endproduct. Adaptation of ACOMP to feedback control will yield model independent output signals and input will rely on robust kinetic models based on basic reaction principles rather than empirical correlations. Anomalies, such as microgelation, massive cross-linking, initiator dead-end, etc., can be monitored as they occur, without reliance on inferential models [71,72].

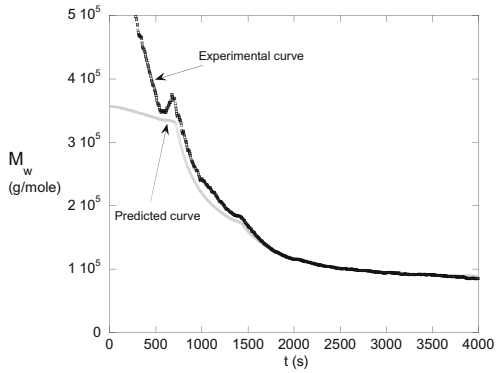

Fig. 11. M_w vs. t when two initiator boosts are made. The gray scale curve is the predicted behavior for M_w vs. t (not a fit).

As polymeric materials become more sophisticated in their functions, such as the ability to self-heal and to respond to external stimuli, the possibility of producing specific, highly tailored polymers 'on-command' is very promising.

While semi-batch protocols are frequently used for controlling composition drift in free radical copolymerization reactions, the current work sets the stage for simultaneous control of both composition and molecular weight in such reactions. In fact, there are several natural directions emanating from the approach developed here; molecular weight and composition control in emulsion copolymerization reactions, control of composition gradients in 'living' copolymerization, terpolymerization control, and combining chain transfer agents with predictive control for even greater flexibility over M_w evolution during reactions.

Acknowledgments

The authors acknowledge support from NSF CBET 0623531, Louisiana Board of Regents ITRS RD-B-5, the Tulane Institute for Macromolecular Engineering and Science, NASA NNX08AP04A, and the Tulane Center for Polymer Reaction Monitoring and Characterization (PolyRMC).

References

[1] Florenzano FH, Strelitzki R, Reed WF. Absolute, online monitoring of molar mass during polymerization reactions. Macromolecules 1998;31:7226–38.
[2] Giz A, Giz H, Brousseau J-L, Alb AM, Reed WF. Kinetics and mechanism of acrylamide polymerization by absolute, online monitoring of polymerization kinetics. Macromolecules 2001;34:1180–91.
[3] Richards JR, Congalidis JP. Measurement and control of polymerization reactors. Comp Chem Eng 2006;30(10–12):1447–63.

[4] Richards JR, Congalidis JP. Measurement and control of polymerization reactors. In: Meyer T, Keurentjes J, editors. Handbook of polymer reaction engineering. Weinheim, Germany: Wiley-VCH; 2005. p. 595–678.
[5] Liptak BG. Instrument engineer's handbook. In: Process measurement and analysis, 4th ed. New York: CRC Press, 2003.
[6] Rodriguez F, Cohen C, Ober C, Archer LA. Principles of polymer systems. 5th ed. New York: Taylor and Francis; 2003.
[7] Kammona O, Chatzi EG, Kiparissides C. Recent developments in hardware sensors for the online monitoring of polymerization reactions. J Macromol Sci – Rev Macromol Chem 1999;C39(1): 57–134.
[8] Hammouri H, McKenna TF, Othman S. Applications of nonlinear observers and control: improving productivity and control of free radical solution copolymerization. Ind Eng Chem Res 1999;38(12): 4815–24.
[9] Dochain D, Pauss A. On-line estimation of microbial specific growth rates: an illustrative case study. Can. J. Chem. Eng. 1988;66(4): 626–31.
[10] Ellis MF, Taylor TW, Jensen KF. Online molecular weight distribution estimation and control in batch polymerization. AIChE J 1994;40(3):445–62.
[11] Kozub DJ, MacGregor JF. State estimation for semi-batch polymerization reactors. Chem. Eng. Sci. 1992;47(5):1047–62.
[12] Mutha RK, Cluet WR, Penlidis A. Online nonlinear model-based estimation and control of a polymer reactor. AIChE J 1997;43(11): 3042–58.
[13] Mutha RK, Cluet WR, Penlidis A. A new multirate-measurement-based estimator: emulsion copolymerization batch reactor case study. Ind Eng Chem Res 1997;36(4):1036–47.
[14] Fevotte G, McKenna TF, Othman S, Hammouri H. Non-linear tracking of glass transition temperatures for free radical emulsion copolymers. Chem Eng Sci 1998;53(4):773–86.
[15] Othman S, Barudio I, Fevotte G, McKenna TF. Online monitoring and modeling of free radical copolymerizations: butyl acrylate/vinyl acetate. Polym React Eng 1999;7(1):1–42.
[16] Kravaris C, Wright RA, Carrier JF. Nonlinear controllers for trajectory tracking in batch processes. Comp Chem Eng 1989;13(1–2):73–82.
[17] Alhamad B, Romagnoli JA, Gomes VG. On-line multi-variable predictive control of molar mass and particle size distributions in free-radical emulsion copolymerization. Chem Eng Sci 2005;60(23): 6596–606.
[18] Garcia CE, Morari M. Internal model control. A unifying review and some new results. Ind Eng Chem Process Des Dev 1982;21(2):308–23.
[19] Park M-J, Rhee H-K. Control of copolymer properties in a semibatch methyl methacrylate/methyl acrylate copolymerization reactor by using a learning-based nonlinear model predictive controller. Ind Eng Chem Res 2004;43(11):2736–46.
[20] Gattu G, Zafiriou E. Nonlinear quadratic dynamic matrix control with state estimation. Ind Eng Chem Res 1992;31(4):10961104.
[21] Lee JH, Ricker NL. Extended Kalman filter based nonlinear model predictive control. Ind Eng Chem Res 1994;33(6):1530–41.
[22] Henson MA. Nonlinear model predictive control: current status and future directions. Comp Chem Eng 1998;23(2):187–202.
[23] Parouti S, Kammona O, Kiparissides C, Bousquet J. A comprehensive experimental investigation of the methyl methacrylate/butyl acrylate/acrylic acid emulsion terpolymerization. Polym React Eng 2003;11(4):829–53.
[24] Cao GP, Zhu ZN, Zhang MH, Le HH. Molecular weight distribution of poly(methyl methacrylate) produced in a starved feed reactor. J Polym Eng 2001;21(5):401–19.
[25] Aerdts AM, Theelen SJC, Smit TMC, German AL. Grafting of styrene and methyl methacrylate concurrently onto polybutadiene in semicontinuous emulsion processes and determination of copolymer microstructure. Polymer 1994;35(8):1648–53.
[26] Wu J-Y, Shan G-R. Kinetic and molecular weight control for methyl methacrylate semi-batch polymerization. I. Modelling. J Appl Polym Sci 2006;100(4):2838–46.
[27] Hur S-M, Park M-J, Rhee H-K. Design and application of model-on-demand predictive controller to a semibatch copolymerization reactor. Ind Eng Chem Res 2003;42(4):847–59.
[28] Sun X, Luo Y, Wang R, Li B-G, Liu B, Zhu S. Programmed synthesis of copolymer with controlled chain composition distribution via semibatch RAFT copolymerization. Macromolecules 2007;40(4): 849–59.
[29] Wang R, Luo Y, Li B, Sun X, Zhu S. Design and control of copolymer composition distribution in living radical polymerization using semi-batch feeding policies: a model simulation. Macromol Theory Simul 2006;15(4):356–68.
[30] Vicente M, Leiza JR, Asua JM. Simultaneous control of copolymer composition and MWD in emulsion copolymerization. AIChE J 2001;47(7):1594–606.
[31] Vicente M, Sayer C, Leiza JR, Arzamendi G, Lima EL, Pinto JC, Asua JM. Dynamic optimization of non-linear emulsion copolymerization systems. Open-loop control of composition and molecular weight distribution. Chem Eng J 2002;85(2–3):339–49.
[32] Yanjarappa JM, Gujraty KV, Joshi A, Saraph A, Kane RS. Synthesis of copolymers containing an active ester of methacrylic acid by RAFT: controlled molecular weight scaffolds for biofunctionalization. Biomacromolecules 2006;7(5):1665–70.
[33] Asua JM. Introduction to polymerization processes. In: Asua JM, editor. Polymer reaction engineering. Oxford: Blackwell Publishing Ltd.; 2007. p. 1–28.
[34] Kiparissides C, Morris J. Intelligent manufacturing of polymers. Comp Chem Eng 1996;20:1113–8.
[35] Dimitratos J, Georgazkis C, El-Aasser MS, Klein A. Dynamic modeling and state estimation for an emulsion copolymerization reactor. Comp Chem Eng 1989;13(1–2):21–33.
[36] Congalidis JP, Richards JR, Ray WH. Feedforward and feedback control of a solution copolymerization reactor. AIChE J 1989;35(6):891–907.
[37] Clay PA, Gilbert RG. Molecular weight distributions in free-radical polymerizations. 1. Model development and implications for data interpretation. Macromolecules 1995;28(2):552–69.
[38] Ghielmi A, Storti G, Morbidelli M. Molecular weight distribution in emulsion polymerization: role of active chain compartmentalization. Macromolecules 1998;31(21):7172–86.
[39] Othman NS, Fevotte G, Peycelon D, Egraz J-B, Suau J-M. Control of polymer molecular weight using near infrared spectroscopy. AIChE J 2004;50(3):654–64.
[40] Adebekun D, Schorl FJ. Continuous solution polymerization reactor control. 2. Estimation and nonlinear reference control during methyl methacrylate polymerization. Ind Eng Chem Res 1989;28(12): 1846–61.
[41] Modi PJ, Guillet JE. Photochemical control of molecular weight during free-radical polymerization. Macromolecules 1994;27(12): 3319–21.
[42] Clarke-Pringle T, MacGregor JF. Nonlinear adaptive temperature control of multi-product, semi-batch polymerization reactors. Comp Chem Eng 1997;21(12):1395–409.
[43] Garcia CE, Morari M. Optimal operation of integrated processing systems. Part II: closed-loop on-line optimizing control. AIChE 1984;30(2):226–34.
[44] Giz A, Koc AO, Catalgil-Giz H, Alb AM, Reed WF. Online monitoring of composition, sequence length, and molecular weight distributions during free radical copolymerization, and subsequent determination of reactivity ratios. Macromolecules 2002;35(17):6557–71.
[45] Mignard E, Leblanc T, Bertin D, Guerret O, Reed WF. Online monitoring of controlled radical polymerization: nitroxide-mediated gradient copolymerization. Macromolecules 2004;37(3):966–75.
[46] Dotson NA, Galvan R, Laurence RL, Tirrel M. Polymerization process modeling. New York: VCH Publishers; 1995.
[47] Kreft T, Reed WF. Direct monitoring of the cross-over from diffusion-controlled to decomposition-controlled initiation in free radical polymerization. Macromol Chem Phys 2008;209(24):2463–74.
[48] Kuchta F-D, Van Herk AM, German AL. Propagation kinetics of acrylic and methacrylic acid in water and organic solvents studied by pulsed-laser polymerization. Macromolecules 2000;33(10): 3641–9.
[49] Ganachaud F, Balic R, Monteiro MJ, Gilbert RG. Propagation rate coefficient of poly(*N*-isopropylacrylamide) in water below its lower critical solution temperature. Macromolecules 2000;33(23): 8589–96.
[50] Beuermann S, Buback M, Hesse P, Lacik I. Free-radical propagation rate coefficient of nonionized methacrylic acid in aqueous solution from low monomer concentrations to bulk polymerization. Macromolecules 2006;39(1):184–93.
[51] Stach M, Lacik I, Chorvat D, Buback M, Hesse P, Hutchinson RA, Tang L. Propagation rate coefficient for radical polymerization of *N*-vinyl pyrrolidone in aqueous solution obtained by PLP-SEC. Macromolecules 2008;41(14):5174–85.
[52] Beuermann S, Buback M, Hesse P, Kuchta F-D, Lacik I, Van Herk AM. Critically evaluated rate coefficients for free-radical polymerization, part 6: propagation rate coefficient of methacrylic acid in aqueous solution: (IUPAC technical report). Pure Appl Chem 2007;79(8): 1463–9.
[53] Beuermann S, Buback M, Hesse P, Hutchinson RA, Kukuckova S, Lacik I. Termination kinetics of the free-radical polymerization of

nonionized methacrylic acid in aqueous solution. Macromolecules 2008;41(10):3513–20.
[54] Pascal P, Winnik MA. Pulsed laser study of the propagation kinetics of acrylamide and its derivatives in water. Macromolecules 1993;26(17):4572–6.
[55] Seabrook SA, Tonge MP, Gilbert RG. Pulsed laser polymerization study of the propagation kinetics of acrylamide in water. J Polym Sci A: Polym Chem 2005;43(7):1357–68.
[56] Seabrook SA, Pascal P, Tonge MP, Gilbert RG. Termination rate coefficients for acrylamide in the aqueous phase at low conversion. Polymer 2005;46(23):9562–73.
[57] Blackley DC, Andries S, Sebastian RD. Effects of inorganic electrolytes upon emulsion polymerization reactions. I. Effects upon kinetics of styrene emulsion homopolymerization and of styrene–acrylic acid emulsion copolymerization. Br. Polym. J. 1989;21(4):313–26.
[58] Lacik I, Beuermann S, Buback M. PLP-SEC study into free-radical propagation rate of nonionized acrylic acid in aqueous solution. Macromolecules 2003;36(25):9355–63.
[59] Lacik I, Beuermann S, Buback M. PLP-SEC study into the free-radical propagation rate coefficients of partially and fully ionized acrylic acid in aqueous solution. Macromol Chem Phys 2004;205(8):1080–7.
[60] Seabrook SA, Gilbert RG. Photo-initiated polymerization of acrylamide in water. Polymer 2007;48(16):4733–41.
[61] Chauvin F, Alb AM, Bertin D, Reed WF. Kinetics and molecular weight evolution during controlled radical polymerization. Macromolecules 2002;203(14):2029–41.
[62] Alb AM, Enohnyaket P, Drenski MF, Head A, Reed AW, Reed WF. Online monitoring of copolymerization involving comonomers of similar spectral characteristics. Macromolecules 2006;39(17): 5705–13.
[63] Giz A, Catalgil-Giz H, Alb AM, Brousseau JL, Reed WF. Kinetics and mechanisms of acrylamide polymerization from absolute, online monitoring of polymerization reaction. Macromolecules 2001;34(5):1180–91.
[64] Norwood DP, Reed WF. Comparison of online single-capillary and bridge capillary viscometric detectors for size exclusion chromatography. Int J Polym Anal Char 1997;4(2):99–132.
[65] Zimm BH. The scattering of light and the radial distribution function of high-polymer solutions. J Chem Phys 1948;16:1093–9.
[66] Mignard E, Guerret O, Bertin D, Reed WF. Automatic continuous online monitoring of polymerization reactions (ACOMP) adapted to high viscosity reactions. PMSE Preprints 2003;88:314–6.
[67] Richardson WH. Bayesian-based iterative method of image restoration. J Opt Soc Am 1972;62:55–9.
[68] Parzen E. Modern probability theory and its applications. New York: Wiley; 1960.
[69] Elizalde O, Asua JM, Leiza JR. Monitoring of high solids content starved-semi-batch emulsion copolymerization reactions by Fourier transform Raman spectroscopy. Appl Spectrosc 2005;59(10): 1270–9.
[70] Reed WF. A method for online monitoring of polydispersity during polymerization reactions. Macromolecules 2000;33(19):7165–72.
[71] Alb AM, Mignard E, Drenski MF, Reed WF. In situ time-dependent signatures of light scattered from solutions undergoing polymerization reactions. Macromolecules 2004;37(7):2578–87.
[72] Farinato RS, Calbick J, Sorci GA, Florenzano FH, Reed WF. Online monitoring of the final, divergent growth phase in the step-growth polymerization of polyamines. Macromolecules 2005;38(4): 1148–58.

Glossary

A: approach index; measures asymptotic approach to steady state
$m_s(t)$: mass (g) of component s in the reactor at any time t
$m(t)$: mass (g) of monomer in the reactor at time t
$m_p(t)$: mass (g) of polymer in the reactor at time t
$m_c(t)$: $m(t) + m_p(t)$ = combined mass of monomer and polymer in the reactor; i.e. the sum of initial monomer in reactor plus monomer flowed into the reactor, minus the amount flowed out into the ACOMP sample stream
c_s: concentration (g/cm^3) of component s in the reactor at time t
c_s': concentration (g/cm^3) of component s in the external reservoir that feeds the reactor
$f(t)$: 'instantaneous' fractional conversion of monomer into polymer at time t (Eq. (22))
$V(t)$: total volume of the reactor contents
$\Delta V_s(t)$: volume of fluid containing component s that has flowed into the reactor by time t
q: constant flow rate (cm^3/s) out of the reactor for the ACOMP extraction stream
$Q_s(t)$: flow rate (cm^3/s) of component s into the reactor at any time.
k_d: initiator dissociation constant (s^{-1})
k_i: initiation rate coefficient (L/M s units)
k_t: termination rate coefficient (L/M s units)
k_p: propagation rate coefficient
α: first-order propagation rate constant (s^{-1}) = $k_p R\bullet$
F: fraction of decomposed radicals, $I\bullet$, which go on to initiate radicals $R_1\bullet$
M_w: weight average molecular weight
$M_{w,inst}$: instantaneous weight average molecular weight
w: instantaneous polydispersity, $M_{w,inst}/M_{n,inst}$
$[\eta]_w$: weight average intrinsic viscosity

All molar quantities (M/L) are expressed with square brackets; e.g.
$[s]$: molar concentration of component s
$[s]'$: molar concentration of component s in external reservoir feeding into the reactor
$[m_m]$: molar concentration of monomer
$[I_2]$: molar concentration of initiator
v_s: conversion factor from molar to CGS concentration units ($c_s = v_s[s]$)